

DOI: [10.29026/oes.2025.240037](https://doi.org/10.29026/oes.2025.240037)CSTR: [32246.14.oes.2025.240037](https://cstr.cn/32246.14.oes.2025.240037)

Aberration-corrected differential phase contrast microscopy with annular illuminations

Yao Fan^{1,2,3†}, Chenyue Zheng^{1,2,3†}, Yefeng Shu^{1,2,3}, Qingyang Fu^{1,2,3},
Lixiang Xiong^{1,2,3}, Guifeng Lu^{1,2,3}, Jiasong Sun^{1,2,3*}, Chao Zuo^{1,2,3*} and
Qian Chen^{1,2,3*}

¹Smart Computational Imaging Laboratory (SCILab), School of Electronic and Optical Engineering, Nanjing University of Science and Technology, Nanjing 210094, China; ²Smart Computational Imaging Research Institute (SCIRI) of Nanjing University of Science and Technology, Nanjing 210019, China; ³Jiangsu Key Laboratory of Visual Sensing & Intelligent Perception, Nanjing 210094, China.

[†]These authors contributed equally to this work.

*Correspondence: JS Sun, E-mail: sunjiasong@njust.edu.cn; C Zuo, E-mail: zuochao@njust.edu.cn; Q Chen, E-mail: chenqian@njust.edu.cn

This file includes:

Section 1: Derivation of the phase transfer function of the complex pupil under differential phase contrast (DPC) for partially coherent imaging

Section 2: Natural exponential decay strategy

Section 3: Data redundancy analysis of the artifact-free aberration-corrected DPC (ACDPC) algorithm

Section 4: Comparison of reconstruction results for gradient descent reconstruction and ACDPC

Supplementary information for this paper is available at <https://doi.org/10.29026/oes.2025.240037>



Open Access This article is licensed under a Creative Commons Attribution 4.0 International License.

To view a copy of this license, visit <http://creativecommons.org/licenses/by/4.0/>.

© The Author(s) 2025. Published by Institute of Optics and Electronics, Chinese Academy of Sciences.

Section 1: Derivation of the phase transfer function of the complex pupil under differential phase contrast (DPC) for partially coherent imaging

Differential phase contrast imaging (DPC), a technique with partially coherent imaging, employs asymmetric half-circular illumination to sequentially illuminate the sample, capturing two phase contrast images for each shearing direction. This method is predicated on the assumption that the complex transmittance function of the object is represented by $t(\mathbf{x}) = e^{i\phi(\mathbf{x})}$, and the tilted illumination light at each angle is denoted by $S(\mathbf{u}_j)$. Here, $\mathbf{x} = (x, y)$ signifies the spatial coordinates within the sample plane, while $\phi(\mathbf{x})$ also denotes the phase components of the sample. To simplify the analysis and isolate the sample's phase and intensity, a weak phase approximation, which requires that the phase perturbation of the sample to the incident light be sufficiently weak, is applied to the complex amplitude distribution of the sample, yielding^{S1,S2}:

$$t(\mathbf{x}) = e^{i\phi(\mathbf{x})} \approx 1 + i\phi(\mathbf{x}) . \quad (\text{S1})$$

Consequently, this leads to the intensity spectrum distribution within the camera plane:

$$I_j(\mathbf{u}) = \iint S(\mathbf{u}_j) \delta(\mathbf{u}) |P(\mathbf{u})|^2 + iS(\mathbf{u}_j) \Phi(\mathbf{u}) [P^*(\mathbf{u}_j)P(\mathbf{u}_j + \mathbf{u}) - P(\mathbf{u}_j)P^*(\mathbf{u}_j - \mathbf{u})] d^2\mathbf{u}_j , \quad (\text{S2})$$

here \mathbf{u} represent the frequency components, and \mathbf{u}_j denote the corresponding phase shifts associated with a single angular illumination. The pupil function, symbolized by $P(\mathbf{u})$, ideally serves as a low-pass filter characterized by a cut-off frequency NA_{obj}/λ , permitting only the frequency components within the numerical aperture (NA) of the objective lens to pass through. Furthermore, the intensity spectrum distribution in Eq. S2 can be decomposed into two terms:

$$I(\mathbf{u}) = B\delta(\mathbf{u}) + i\Phi(\mathbf{u})\text{PTF}(\mathbf{u}) , \quad (\text{S3})$$

where B represents the background term, computed with $B = \iint S(\mathbf{u}_j) |P(\mathbf{u}_j)|^2 d^2\mathbf{u}_j$, and $\Phi(\mathbf{u})$ is the phase spectrum of the sample. The phase transfer function (PTF) is denoted as:

$$\text{PTF}(\mathbf{u}) = \iint S(\mathbf{u}_j) [P^*(\mathbf{u}_j)P(\mathbf{u}_j + \mathbf{u}) - P(\mathbf{u}_j)P^*(\mathbf{u}_j - \mathbf{u})] d^2\mathbf{u}_j . \quad (\text{S4})$$

This equation serves as a comprehensive expression for the PTF under partially coherent illumination, and it is universally applicable to a variety of illumination functions $S(\mathbf{u})$ and pupil functions $P(\mathbf{u})$.

DPC employs differential computation to filter out the DC component from the intensity signal, thereby retaining solely the phase component associated with the object. Thus, the expression for the corresponding PTF is formulated as follows (presented here as an illustrative example for the left and right shear directions)^{S3,S4}:

$$\text{PTF}_{\text{lr}}(\mathbf{u}) = \frac{\iint S_{\text{lr}}(\mathbf{u}_j) [P^*(\mathbf{u}_j)P(\mathbf{u}_j + \mathbf{u}) - P(\mathbf{u}_j)P^*(\mathbf{u}_j - \mathbf{u})] d^2\mathbf{u}_j}{\iint |S_{\text{lr}}(\mathbf{u}_j)| |P(\mathbf{u}_j)|^2 d^2\mathbf{u}_j} . \quad (\text{S5})$$

This formula reveals that the PTF is determined by the illumination function and the pupil function. These two factors inspired two modulations, namely illumination modulation and optical pupil modulation, to achieve optimization of the PTF and thus enhancement of the imaging performance.

Previous studies have usually used an idealized pupil function to facilitate the calculation of the PTF, whereby it can be considered as a shifted superposition of centrally symmetric sub-apertures. Within the overlapping region of the pupil, opposing values neutralize each other, resulting in a 0-value transfer response. This phenomenon explains the small value of the PTF at the central low frequencies corresponding to conventional DPC half-circular illumination. Over the past few years, some investigative efforts have been dedicated to enhancing the PTF response through optimized illumination strategies^{S5}, such as gradient illumination, radial illumination, etc. We proposed that the optimal illumination pattern is half-annular illumination, where the illumination NA is matched to the objective lens NA and the illumination intensity varies cosinusoidally according to angle^{S6}. Such an illumination configuration yields an isotropic and markedly improved PTF response across both low and high frequencies.

In actual imaging systems, the pupil function deviates from the ideal low-pass filter due to the presence of aberrations. It is characterized by a complex distribution, where the amplitude component manifests as a circular function with a uniform value of 1, and the phase component represents a complex superposition encompassing multiple orders

of aberrations. The PTF deviates from the central symmetry under ideal conditions, exhibiting a more intricate numerical distribution. Consequently, the aberration retrieval in partially coherent imaging modalities poses a significant challenge due to the complexity introduced by these aberrations.

Section 2: Natural exponential decay strategy

We design a learning rate decay strategy based on natural exponential decay to optimize the search process. It uses a large perturbation range is used initially to facilitate extensive search space exploration, while at a later stage, a fine search is implemented and convergence is accelerated by rapidly reducing the perturbation range:

$$D_{\max} = b \left[1 - \exp \left(-\gamma \frac{f}{f_{\max}} \right) \right], \quad (\text{S6})$$

D_{\max} denotes the maximum range of random perturbations, i.e., random perturbations are generated between $[-D_{\max}, D_{\max}]$. b denotes the desirable maximum value of D_{\max} , which we set to 0.4. The term f/f_{\max} represents the value of the normalized cost function, which implicitly has to decrease with the reduction of residuals, and is used to control the attenuation of the maximum range of perturbations. γ is the attenuation coefficient, which is used to control the attenuation rate of the maximum perturbation range, and is set to 2. As the annealing process proceeds, the perturbation range decreases according to a natural exponential function, ensuring faster convergence to the optimal solution while still retaining adequate search capability.

Section 3: Data redundancy analysis of the artifact-free aberration-corrected DPC (ACDPC) algorithm

The conventional DPC technique acquires four images for deconvolution reconstruction with sufficient redundancy of data information to ensure correct inversion of object amplitude and phase. However, retrieving the aberration from the raw data provides a greater data requirement for DPC reconstruction.

We further explore the minimum data acquisition scheme of ACDPC for simultaneous aberration retrieval and phase reconstruction. The simulation results of the ACDPC method for different components of the complex amplitude (Amplitude and phase) of the object and the system aberration reconstruction task are presented in Fig. S1, respectively. We used a USAF resolution target as the amplitude and phase to construct the complex transmittance function of the object and generated random pupil function, which were used to generate the acquisition intensity images. Figure S1(b) gives the reconstructed phase comparisons of DPC and ACDPC for two images, three images, and four images. It can be noticed that they all correct the aberration and give a clear, artifact-free reconstructed phase. The detailed comparison in Fig. S1(b) shows that they achieve a theoretical resolution of 345 nm at the imaging parameters (The simulation parameters are described in the simulation results for different aberrations).

To demonstrate the capability of the ACDPC method to deal with complex problems, the three key tasks of reconstructing the amplitude, phase and retrieving the phase are further performed, and Fig. S1(c) displays the reconstruction results. With four raw acquisitions, ACDPC can simultaneously recover the amplitude and phase of the object and retrieve the pupil aberration that conforms to the ground truth, realizing high-quality object information reconstruction.

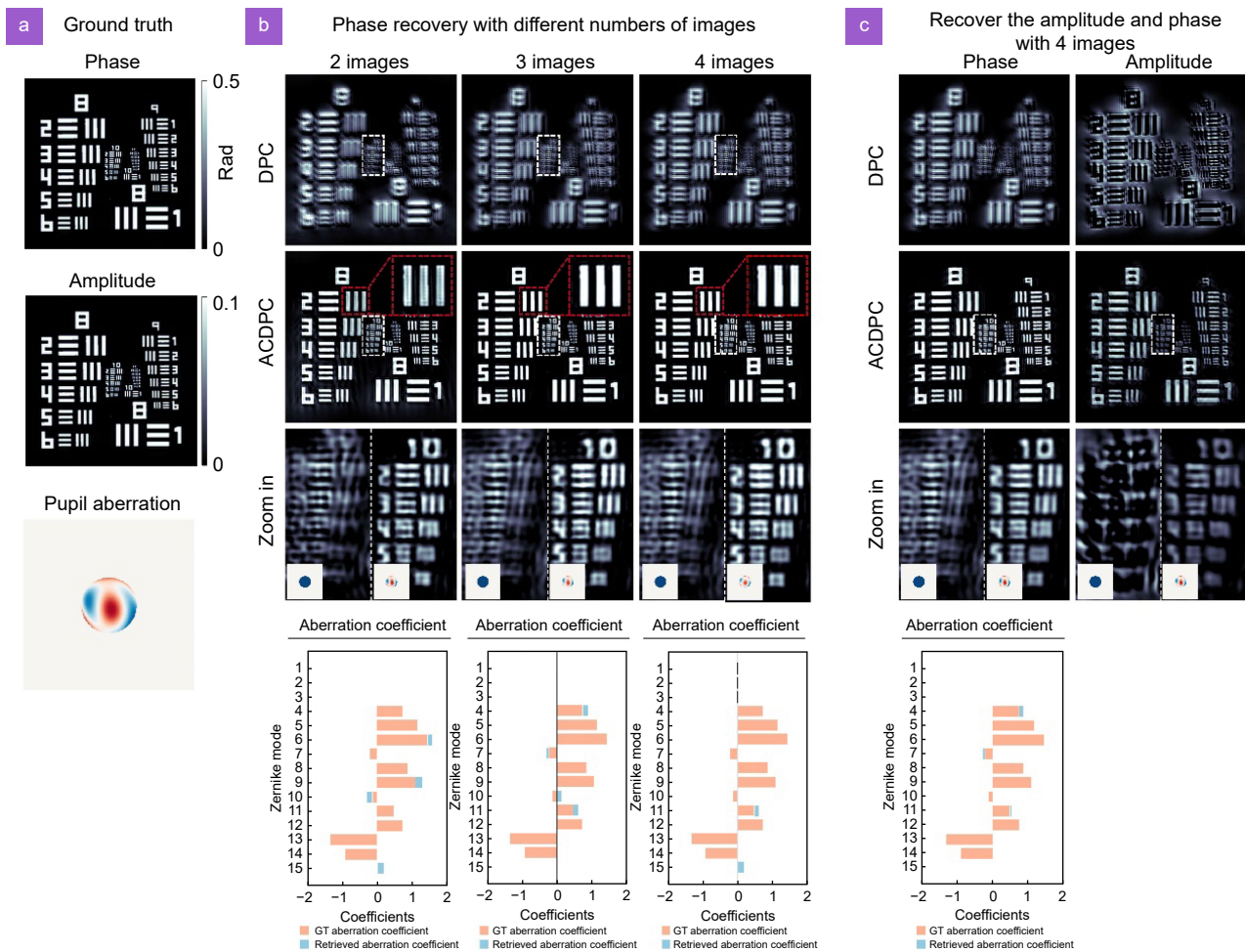


Fig. S1 | Comparison of DPC and ACDPC reconstruction results with different data redundancy. (a) Ground-truth (GT) amplitude, phase, and pupil distribution for simulation. (b) Reconstruction phase of DPC and ACDPC methods with different raw data (Two images, three images, and four images). (c) Reconstruction amplitude and phase of DPC and ACDPC methods with 4 raw images.

Section 4: Comparison of reconstruction results for gradient descent reconstruction and ACDPC

In previous work, gradient descent methods have been proposed for aberration correction of DPC. Chen et al.^{S7} used three raw intensity images acquired with semicircular illumination and one with single-point illumination to jointly recover the phase and absorption of the samples as well as to estimate the systematic aberration via a gradient descent algorithm. This method takes the residuals of the acquired and generated intensities as a cost function and updates the aberration and phase based on the inverse direction of their gradients (i.e., derivatives) so that they progressively approximate the optimal solution. While the gradient descent method exhibits robust performance in optimizing convex models, it is susceptible to converging to local minima when applied to non-convex optimization problems such as partially coherent imaging model. We use simulation to compare the aberration correction performance of the gradient descent method with the ACDPC method.

As depicted in Fig. S2, we introduced randomly generated aberration into the pupil and employed the Abbe model to synthesize the raw images for the gradient descent method and ACDPC. The original image for the gradient descent method consists of intensity images taken under three half-circular illuminations and one image under a single point illumination, while the ACDPC contains intensity images under three half-annular illuminations. The specimen was configured as a USAF resolution target, characterized by a phase of 0–0.5 rad, and it was illuminated by a light source with a wavelength of 525 nm. The light field data were collected using a 20× objective lens with a NA of 0.4 and projected onto a sensor with a pixel size of 1.85 μm . Figure S2(a) presents a comparative analysis of the reconstructions between the gradient descent method and the ACDPC method. The aberration estimated by the gradient descent method deviates

from the actual aberration values, resulting in a phase with significant artifacts.

Particularly, the high-frequency components exhibit severe distortions, failing to achieve the theoretical resolution limit. This observation suggests that the iterative process of the method tends to converge to local minima. Extensive simulation experiments have demonstrated that the gradient descent method generally yields superior results in the majority of scenarios, with the exceptions highlighted in Fig. S2(a). Nevertheless, this result underscores the limitations of the gradient descent method in aberration correction for partially coherent imaging. In contrast, ACDPC method retrieves a clear and precise QPI through a global optimization approach, with the estimated aberration closely matching the GT aberration.

This simulation indicates that ACDPC method effectively circumvents the pitfalls of local minima and consequently enhancing image quality compared to the gradient descent method.

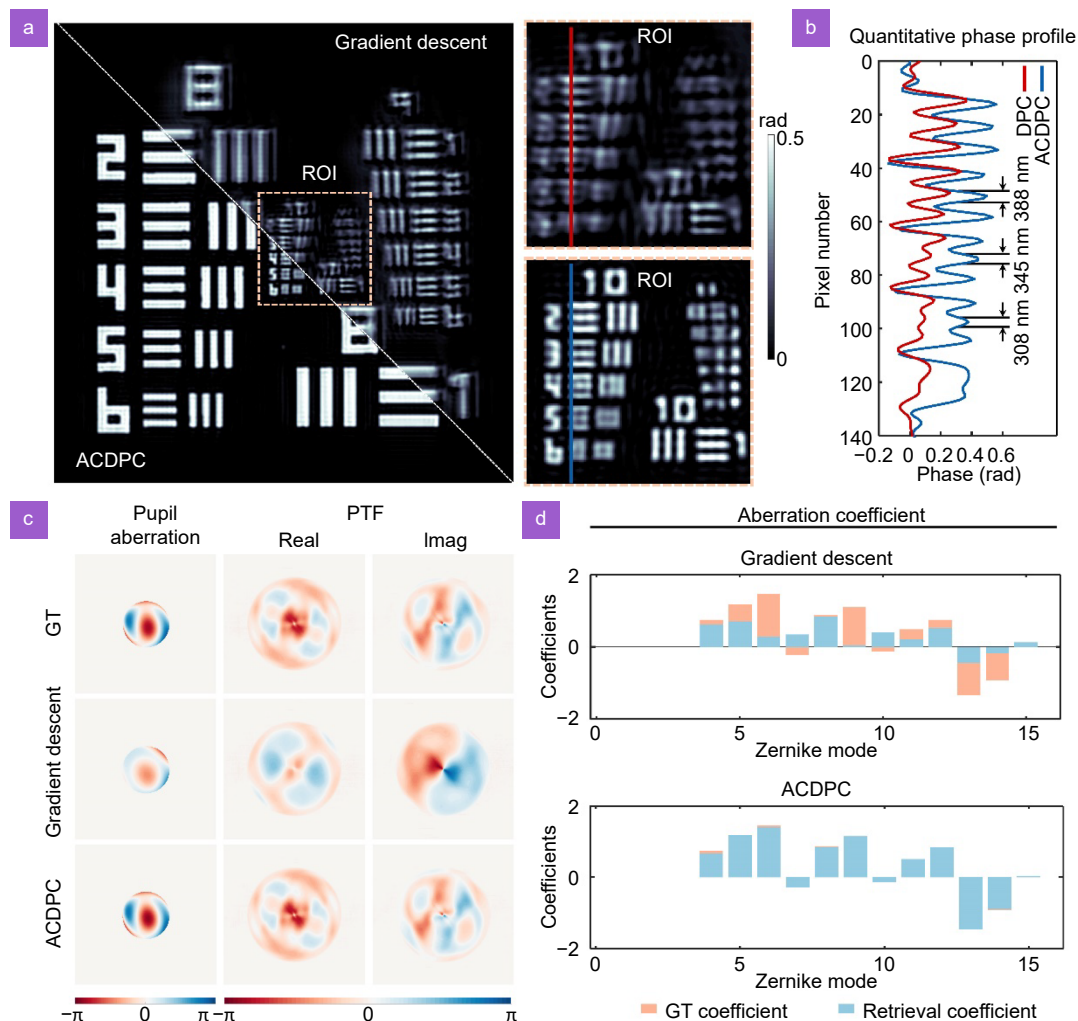


Fig. S2 | Comparison of gradient descent method and ACDPC reconstruction results. (a) Reconstruction phase of gradient descent and ACDPC methods. (b) Comparison of the GT pupil and the corresponding PTF with the retrieved pupil and PTF by gradient descent and ACDPC. (c) Comparison of aberration coefficients for GT aberration and retrieval aberration of gradient descent and ACDPC. (d) Aberration coefficient of retrieved by gradient descent and ACDPC methods.

References

- S1. Hamilton DK, Sheppard CJR. Differential phase contrast in scanning optical microscopy. *J Microsc* **133**, 27–39 (1984).
 S2. Mehta SB, Sheppard CJR. Quantitative phase-gradient imaging at high resolution with asymmetric illumination-based differential phase contrast. *Opt Lett* **34**, 1924–1926 (2009).

- S3. Tian L, Waller L. Quantitative differential phase contrast imaging in an led array microscope. *Opt Express* **23**, 11394–11403 (2015).
- S4. Fan Y, Sun JS, Shu YF et al. Accurate quantitative phase imaging by differential phase contrast with partially coherent illumination: beyond weak object approximation. *Photon Res* **11**, 442–455 (2023).
- S5. Chen HH, Lin YZ, Luo Y. Isotropic differential phase contrast microscopy for quantitative phase bio-imaging. *J Biophoton* **11**, e201700364 (2018).
- S6. Fan Y, Sun JS, Chen Q et al. Optimal illumination scheme for isotropic quantitative differential phase contrast microscopy. *Photon Res* **7**, 890–904 (2019).
- S7. Chen M, Phillips ZF, Waller L. Quantitative differential phase contrast (DPC) microscopy with computational aberration correction. *Opt Express* **26**, 32888–32899 (2018).